Compact, Monolithically 3-D-Printed, Hyperbolic Quadrupole Mass Filters for CubeSat Mass Spectrometry

Alejandro Diaz and Luis Fernando Velásquez-García, *Senior Member, IEEE*

***Abstract*— We report the design, fabrication, and characterization of monolithically 3-D-printed, hyperbolic, compact RF quadrupole mass filters (QMFs) for CubeSat mass spectrometry (MS). The devices are fabricated via multimaterial extrusion using polylactic acid (PLA) for the dielectric parts and PLA doped with copper nanoparticles for the conductive parts. The work also included the development of compact electronics to drive the QMFs that are compatible with the size, weight, and power constraints of CubeSats. Experimental characterization shows the QMFs can scan up to 300 Da of mass range and can satisfactorily generate mass spectra for argon (a representative gas found in the ionosphere). The work is of interest for in-space manufacturing of CubeSat chemical sensors that could expand our understanding of climate change and atmospheric pollution.**

***Index Terms*— Additively manufactured chemical sensors, compact mass spectrometry (MS), CubeSat instrumentation, low-power electronics, multimaterial extrusion, quadrupole mass filter (QMF).**

I. Introduction

MASS spectrometry (MS) is the gold standard for quantitative chemical analysis. Mass spectrometers employ mass filters that use electromagnetic fields to sort out, in vacuum, by mass-to-charge ratio, the ionized constituents of a sample [1]. However, mainstream mass spectrometers are bulky, heavy, and power hungry, i.e., they are incompatible with deployment in autonomous platforms, such as drones and CubeSats. However, having such MS data would be invaluable for climate change monitoring and pollution tracking [2]. The CubeSat application has the advantage that it does not require vacuum pumps, simplifying the hardware and greatly reducing the power consumption of the miniaturized mass spectrometer [3]. There are a wide variety of mass filters employed in MS, including magnetic sectors [4], time-of-flight (TOF) [5], ion traps [6], and quadrupoles [7]. Nonetheless, many of these mass filters are hard to miniaturize while still attaining adequate performance [8], [9]. For example, magnetic sectors require more powerful magnets to deflect ions of the same energy across smaller regions in space, and TOFs require high-performance electronics to measure increasingly shorter ion flight times.

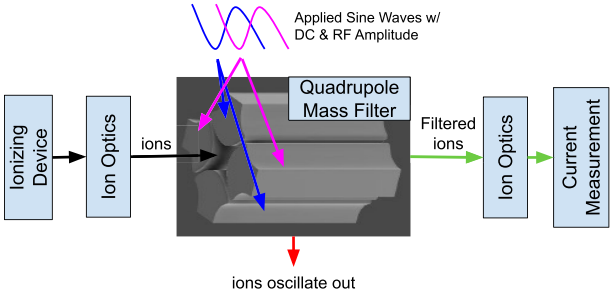

Fig. 1. Schematic of a mass spectrometer with a quadrupole as mass filter. Ion optics direct the ions into the QMF and into the detector.

A quadrupole mass filter (QMF) is composed of four conductive rods symmetrically arranged around an axis that filter ions while being biased at sinusoidal voltages of specific phase, amplitude, and dc offset (see Fig. 1). QMF mass spectrometers are not true mass spectrometers in the sense that they do not sort out all species at the same time. Instead, for a given mix of voltages, they only transmit ions of a certain mass-to-charge ratio. Mass spectra are obtained by assuming the ions are singly ionized and by varying in time (sweeping) the amplitude of the mix of voltages applied to the QMF while measuring the current transmitted by the mass filter at each voltage combination.

The dynamics of ions inside a QMF are described by the Mathieu equation [10]

$$\frac{d^2u}{d\xi^2} + \left[a - 2q\cos(2\xi)\right]u = 0 \tag{1}$$

where u is a spatial coordinate perpendicular to the axis of the quadrupole (e.g., x and y for a quadrupole with z axis) and ξ is a dimensionless parameter equal to $\omega \cdot t/2$, where t is time and ω is the angular frequency of the RF voltage. The stability of the ion trajectories within the quadrupole potential well (i.e., whether the ions are transmitted across the

Manuscript received 19 January 2024; accepted 19 February 2024. Date of publication 1 March 2024; date of current version 14 March 2024. This work was supported in part by the NewSat Project through the Operational Program for Competitiveness and Internationalization (COMPETE2020), Portugal 2020; in part by the European Regional Development Fund (ERDF); and in part by the Portuguese Foundation for Science and Technology (FTC) through the Massachusetts Institute of Technology (MIT) Portugal Program. The Associate Editor coordinating the review process was Dr. Ada Fort First. *(Corresponding author: Luis Fernando Velásquez-García.)*

Alejandro Diaz is with the Department of Electrical Engineering and Computer Science, Massachusetts Institute of Technology, Cambridge, MA 02465 USA (e-mail: addiaz15@mit.edu).

Luis Fernando Velásquez-García is with the Microsystems Technology Laboratories, Research Laboratory of Electronics, Massachusetts Institute of Technology, Cambridge, MA 02139 USA (e-mail: Velasquez@alum.mit.edu).

Digital Object Identifier 10.1109/TIM.2024.3372214

QMF to the detector) depends on the values of the associated dimensionless parameters a and q, which is given by

$$a = \frac{8eU}{mr_o^2\omega^2} \tag{2}$$

$$q = \frac{4eV}{mr_o^2\omega^2} \tag{3}$$

where U is the dc offset, V is the amplitude of the RF voltage, e is the electron's charge, m is the mass of the ion, and r_o is half the separation between electrodes opposed across the QMF axis. For the first stability region of the Mathieu equation (the stability region at which the great majority of QMFs operate), $a = 0.237$ and $q = 0.706$. For a given (a, q), it is possible to compensate a decrease in the dimensions of the QMF with changes in the frequency and amplitudes of the RF and dc voltages, so ions still have stable trajectories within the mass filter and are transmitted to the detector. Consequently, there are multiple reports of miniaturized QMFs that explore this idea [11], [12], [13], [14]. However, the manufacture of these devices is expensive, time-consuming, and incompatible with current in-space manufacturing capabilities. In addition, some of these designs use nonideal electrode shapes (e.g., square electrodes [13]) that introduce spurious harmonics that greatly affect the mass filter's performance.

Additive manufacturing (AM) encompasses a group of techniques for fabricating solid objects, typically layer by layer, using a computer-aided design (CAD) file as a template [15]. Via AM, it is possible to build freeform objects. Moreover, via material extrusion (an AM technique that creates objects by rastering across a surface a nozzle that pours material [16]), it is possible to monolithically create complex, functional, multimaterial hardware [17], [18], [19]. There are reports of 3-D-printed, miniature QMFs [20], [21], but they are not monolithically made, neither are fully made via 3-D printing. Additionally, extrusion is not only the most widely spread 3-D printing method, but also it uses the cheapest printing hardware and feedstock.

Presently, only chemical rockets can put a payload in orbit [22]. Based on the rocket equation [23], placing a body in orbit requires ejecting many times its mass; therefore, only a small fraction of the rocket is cargo. Currently, the cost to put an object in orbit is on the order of thousands of dollars per kilogram, and the cost of a rocket is on the order of tens of millions of U.S. dollars [24], greatly limiting the kinds of missions that can be implemented in space. The adoption of CubeSats to implement space missions could decisively help reduce costs as they introduce large savings in mass and volume compared to traditional satellites. The cost of space hardware could be further reduced if created in space via AM [26], as it introduces three clear benefits: 1) AM uses multipurpose feedstock, which eliminates the need to have in orbit a stock of parts, e.g., rods of various diameters, plates of various thicknesses, screws, and cables; 2) AM minimizes waste as objects are created net-shape [15]; and 3) any repairs to the hardware do not require shipping spare parts from Earth but can be made in orbit using files transmitted from ground. Furthermore, monolithically 3-D printing hardware saves time and energy during postprinting, e.g., assembly.

Low Earth orbit is currently cluttered with debris from decades of space activity, including orbiting spacecraft not removed at the end of their service life and remnant upper stages from rocket launches [26]. Making space hardware in polymer would greatly facilitate their degradation during reentry. As a matter of fact, there are efforts on making satellites out of wood (i.e., lignin—a polymer) to attain the disposal of the hardware during reentry [27].

This study significantly extends and improves our earlier report of the first proof-of-concept demonstration of compact, monolithically 3-D-printed, hyperbolic RF QMFs [28]. The devices are made via extrusion using polylactic acid (PLA) for the dielectric parts and PLA doped with copper nanoparticles for the conductive parts. The work includes the development of compact, low-power, precision electronics for driving the devices that are compatible with the size, weight, and power constraints of CubeSats. Compared to our earlier report [28], the quadrupoles attain twice the resolution due to improvements in the fabrication of the devices and in the driving circuitry. In particular, the optimized fabrication process attains linearity and close resemblance to the CAD dimensions; moreover, the circuit is capable of delivering twice the voltage while consuming one fourth of the power and generating RF signals with no spurious harmonics. Furthermore, the characterization of the electrical resistance of the conductive material significantly deviates from expected values (from the vendor) but shows that the RF voltages are contained within the electrodes.

II. Device Design

The study developed both a 3-D-printed QMF design and compact electronics to run the QMF.

A. QMF Design

The design of the QMFs reported in this study (see Fig. 2) reflects the capabilities of the 3-D printer employed and the constraints in size and power typically found in a 6U CubeSat. The length of the QMF is 7.5 cm and has four, evenly spaced, electrically isolated, hyperbolic rods separated by 4 mm across the QMF axis (i.e., $r_o = 2$ mm). The shape of the electrodes is motivated by the shape of the equipotential surfaces of the quadrupolar potential, which are hyperbolic. It is possible to implement a QMF with round electrodes, but its performance is significantly lower [29] as it generates spurious harmonics.

To ensure good fabrication accuracy, these dimensions are at least two orders of magnitude larger than the positioning precision of the movement of the 3-D printer ($\sim$25-μm in-plane and $\sim$1-μm out-of-plane—from the vendor). At both ends, the QMF has integrated flanges that mate with standard high-vacuum hardware to greatly facilitate the testing of the QMFs. The QMF is intended to be printed along its axis, from bottom to top. Consequently, the bottom and top flanges have different geometries to interface with the quadrupole dielectric structure to reflect constraints and capabilities associated with 3-D printing via extrusion. Specifically, there is a filleted, 90° transition between the bottom flange and the quadrupole dielectric structure, while there is a 45° transition between the

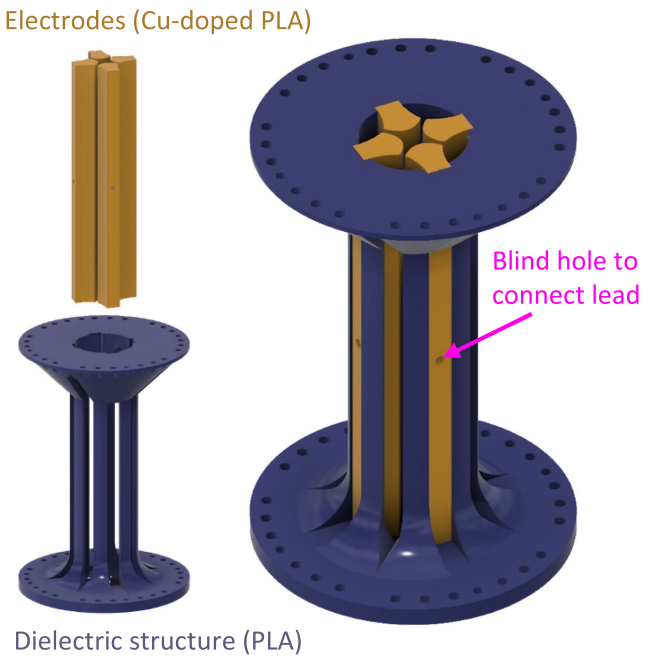

Fig. 2. Exploded CAD view (left) and merged view (right) of the devices reported in this study. In the figure, the nonconductive housing is colored in purple, while the hyperbolic, conductive, electrically isolated rods are colored in gold. Ions are transmitted across the QMF through the space surrounded by the hyperbolic rods.

dielectric structure and the top flange. The 3-D-printed QMFs are designed to be driven at 1–2.65 MHz and use up to 400 V_{PP} to scan a mass range of 1–50 Da, suitable to scan the masses of the gases present in the ionosphere [30]. Each electrode has a blind hole at midpoint of its outermost surface from the axis of the QMF to facilitate connecting leads to the electrodes.

B. Electronics Design

The electronics that drive the QMF need to supply two 180° out-of-phase, RF sinusoidal waves at specific frequencies and amplitudes with dc offsets to be able to transmit ions across the mass filter. The dc offsets for both sinusoidal waves are symmetric about 0 V and opposite. The value of the dc offsets is related to the amplitude of the RF sinusoidal waves as a function of the dimensionless parameters a and q given by (1) and (2) for $(a, q) = (0.237, 0.706)$. The QMF is intended to scan masses between 1 and 50 Da to be able to conduct MS of the ionosphere. Roughly speaking, to accomplish this mass range, the circuit should supply 2–3-MHz RF bias voltages between 4 and 200 V_{pp} with 0.2-V voltage steps and 0.33–16.5-V dc voltage offsets. Alternatively, a lower frequency with a higher voltage range accomplishes the same effect.

In a nutshell, the proposed QMF driving circuit uses full-bridge Class D amplifiers that feed a transformer network and then two series of tunable resistor, inductance, and capacitance (RLC) resonant circuits to energize the QMFs. Amplifiers with Class D topologies were selected because they offer the highest efficiency along with the lowest distortion of the signal [31]. The circuit implements a full-bridge configuration (versus a half-bridge configuration) to achieve higher output power and efficiency despite the added complexity of

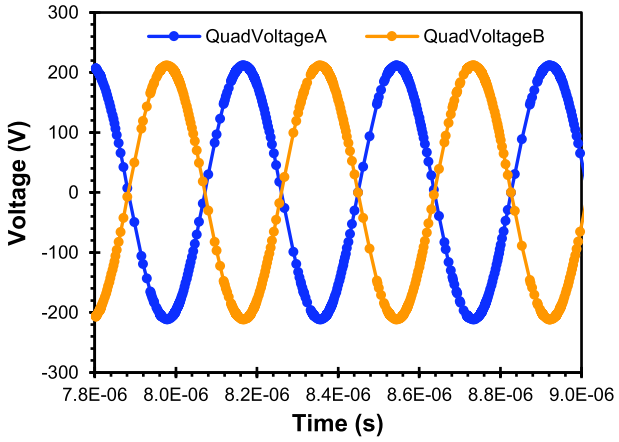

Fig. 3. Simulation result of electromagnetic waves produced by the circuit based on a LTC7060 chip.

the design. The circuits were designed in LTSpice (Analog Devices, Inc., Norwood, MA, USA).

An LTC7060 chip was used to control the pulsewidth modulation (PWM) signals for the four driving MOSFETs part of the bridge, as it only requires a single PWM input, which a microcontroller can easily supply. The full bridge then feeds two parallel transformers that drive two RLC circuits and quadrupole with the sinusoidal waves. The dc voltage applied to the top of the full bridge controls the amplitude of the sinusoidal waves across the quadrupole (the quadrupole is modeled by two capacitors tied to ground). The Fourier analysis of the simulated response of the circuit (see Fig. 3) shows that most of the signal corresponds to a sinusoidal with 2.65-MHz frequency (see Fig. 4). There is a second harmonic around 8 MHz and a third harmonic at about 13 MHz that are an order of magnitude smaller. It is important to produce as much as possible a pure sinusoidal, as higher harmonics affect the capability of the QMF to sort out ions.

III. QMF Fabrication

The QMFs reported in this study were monolithically made via multimaterial extrusion. A modified MakerGear M3-ID (MakerGear LLC, Beachwood, OH, USA) with two independent extruders was used to print the devices using 0.5-mm nozzles and commercial feedstock. Each extruder was dedicated to print a given material to avoid cross-contamination. The dielectric parts of the devices were made in PLA (3-D-Fuel Pro PLA+, 3DomFuel, Inc., Fargo, ND, USA), while the conductive parts were made in PLA doped with copper nanoparticles (Electrifi, Multi3D, Middlesex, NC, USA). Simplify3D (Simplify3D, Cincinnati, OH, USA) was used to slice the CAD files and to finely tune the printing profiles of the materials. The conductive PLA was printed with a nozzle at 160 °C, while the dielectric PLA was printed with a nozzle at 230 °C; in both cases, the bed temperature was set at 65 °C. The devices were printed in 100-μm layers. Leads made of 22 AWG cable were connected to the electrodes using conductive silver epoxy to gain electrical contact to the QMF electrodes.

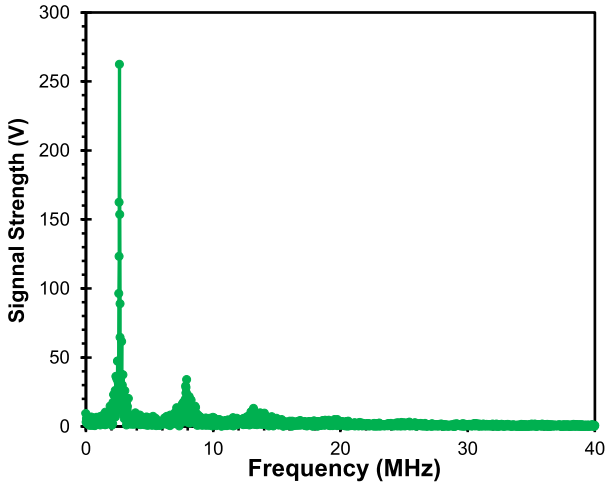

Fig. 4. FFT of the simulated output of the LTC7060 chip-based circuit.

The examples of fabricated devices are shown in Fig. 5. The weight of a QMF with electrical leads connected is about 50 g. Each QMF fits inside a cylinder with 50 mm diameter and 75 mm height (147 cm^3), resulting in a quarter of the maximum mass density of a CubeSat (1.3 kg/L). It takes about 8 h to print a QMF while using about U.S. $100 of printable feedstock—most of the cost is the conductive filament. Given that the QMFs are entirely made of polymer, the devices line up with the aim of producing less junk in space, as disposal of the hardware would take place during CubeSat reentry [35].

IV. Device Characterization and Discussion

The experiments conducted in this study encompassed 1) characterization of the electrical conductivity of the Cu-doped PLA printable feedstock; 2) characterization of the correlation between CAD dimensions and printed dimensions; 3) characterization of the QMF driving electronics; and 4) characterization of the QMFs.

A. Electrical Conductivity Characterization

The experimental characterization of the electrical conductivity of Electrifi was conducted using 3-D-printed structures composed of a long strip on top of a dielectric base, with short copper leads attached every 5 mm using conductive epoxy. The devices were energized using a source-meter power supply (Keithley 2657A, Tektronix, Inc., Beaverton, OR, USA) with 0.03% error when supplying or measuring currents or voltages. The resistance of the copper leads is expected to be insignificant compared to the resistance of the 3-D-printed part (the resistivity of copper is 1.77×10^{-6} $\Omega \cdot$ cm, while the manufacturer of Electrifi reports a resistivity of 6.0×10^{-3} $\Omega \cdot$ cm). Silver epoxy was used to make electrical connection as it has the lowest contact resistance compared to screw terminals or melted Electrifi [32]. To measure the electrical resistivity of 3-D-printed Electrifi, a 0.1-A current was applied to the Electrifi structure, while the voltage was measured relative to ground every 5 mm using the copper leads using a calibrated precision multimeter (Keithley 2100, Tektronix, Inc., Beaverton, OR, USA) with 0.005% voltage measurement

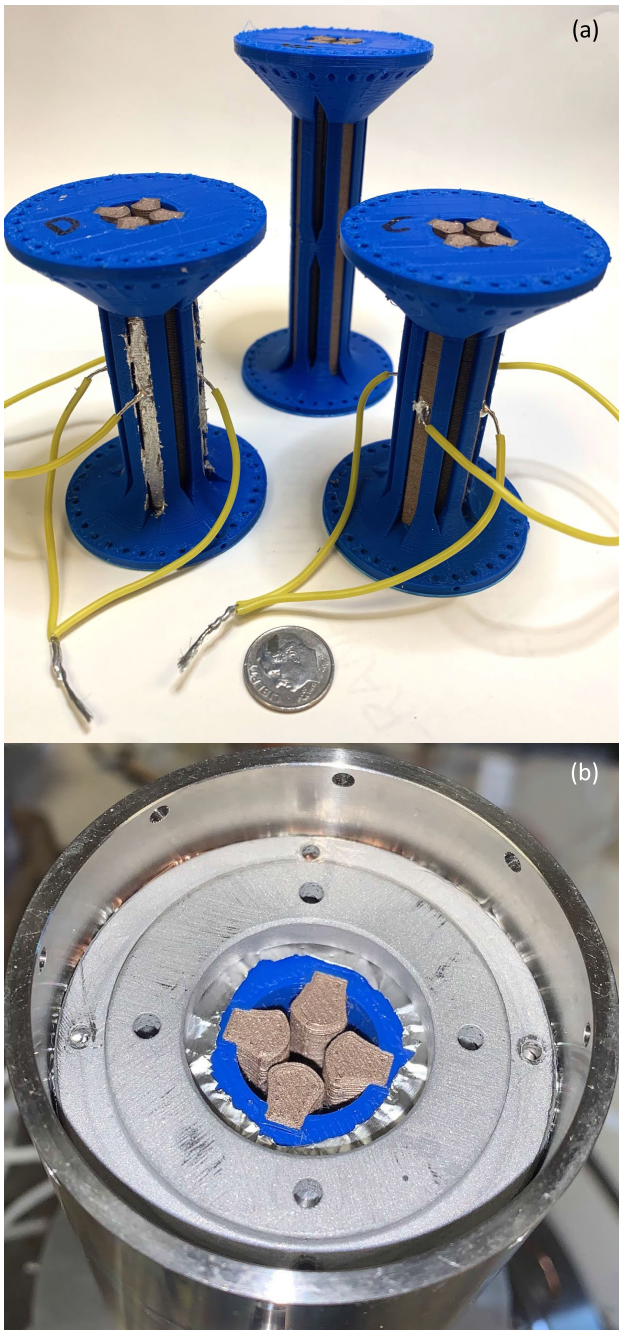

Fig. 5. (a) Monolithically 3-D-printed QMFs next to a U.S. dime coin for comparison. (b) Close-up of QMF inside metal housing (the inner diameter of the metal housing is equal to 5 cm).

error. The structures had a 3 × 5 mm cross section and were printed in 100-μm layers. The electrical resistivity ρ is given by

$$\rho = A\frac{dR_R}{dx} \tag{4}$$

where R_R is the electrical resistance, A is the cross-sectional area of the test structure, and x is the direction along the axis of the structure.

Fig. 6 shows the data from the 3-D-printed test structures used to characterize the electrical resistivity of Electrifi. There is excellent correlation between the data and the linear fit.

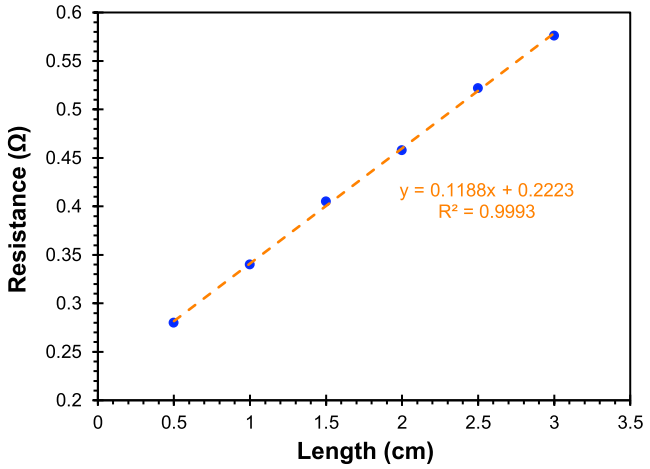

Fig. 6. Resistance versus length from 3-D-printed structures made in Electrifi. The error in the resistance measurements is 0.03%, while the error in the length measurements is 500 μm (the size of the studs printed along the strip that were used to anchor the copper leads).

From the intercept of the fit, a contact resistance equal to 0.11 Ω is obtained; the value corroborates the excellent conductivity of the silver epoxy used to make electrical contact to the 3-D-printed, conductive objects. Similarly, from the slope of the linear fit, the electrical resistivity of Electrifi is estimated at 1.78×10^{-2} Ω.cm. This value is a threefold the resistivity reported by the vendor; however, to the best of our knowledge, it is still by far the smallest resistivity value from a 3-D printable filament [33], [34]. The skin depth σ is given by

$$\sigma = \sqrt{\frac{2\rho}{\pi f \mu_o \mu_r}} \tag{5}$$

where f is the RF frequency, and μ_o and μ_r are the magnetic permeability of free space and the relative magnetic permeability of the material, respectively. Assuming a relative magnetic permeability of 1 for Electrifi results in a skin depth equal to 4.1 mm; in other words, the electrode cross-section is large enough to contain the RF wave (the electrodes are about 10 mm in cross-section).

B. Metrology Results

To assess the fidelity between 3-D-printed and CAD dimensions for each material (PLA, Cu doped PLA), a set of step pyramids that systematically varied the step height and width were made; each step increased 100 μm in height, while the width of the steps decreased by 600 μm. The structures were measured using a confocal microscope with nanometer resolution (Keyence VK-X, Keyence, Itasca, IL, USA).

Table I summarizes the linear fits of the metrology conducted on the step pyramids made of PLA and PLA doped with copper. The linear fit describes the 3-D-printed dimension as a function of the CAD dimension; therefore, for zero CAD dimension, there is an offset in the printed dimension. Following ISO/ASTM 52900:2015 guidelines, X is the in-plane direction that goes from left to right of the printer, Y is the in-plane direction that goes from back to front of the printer, and Z is the out-of-plane direction from bottom to top of the printer.

TABLE I
SUMMARY OF THE LINEAR FITS OF THE METROLOGY DATA CONDUCTED ON 3-D-PRINTED STEP PYRAMIDS

Axis	Material	Measurements	Slope	Offset	R^2
X	3D-Fuel Pro PLA+	2,850	1.0374	-234.48 µm	0.9961
X	Electrifi	2,850	1.0585	-282.12 µm	0.9948
Y	3D-Fuel Pro PLA+	2,700	1.0106	-55.58 µm	0.9988
Y	Electrifi	2,700	0.9881	-34.95 µm	0.9996
Z	3D-Fuel Pro PLA+	18,500	0.9985	-30 µm	0.9995
Z	Electrifi	18,500	0.9768	34.08 µm	0.9881

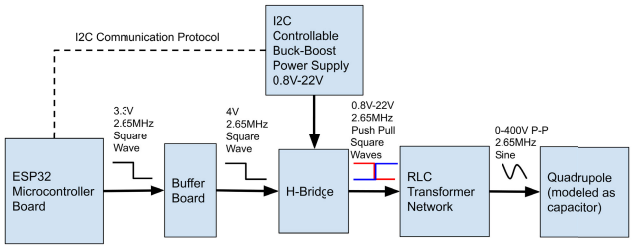

Fig. 7. Block diagram of circuit implemented in this study. Adapted from [28].

Overall, there is excellent correspondence and linearity between the CAD and printed dimensions, in all cases with a least-squares slope close to one. Furthermore, the offsets and slopes of the linear fits are very similar across materials for each axis. However, the offset in the X-axis is larger compared to the offset in the Y-axis—probably a peculiarity of the 3-D printer used in the study given that the XY movement is nominally identical. Following the recommendations of other studies [33], the linear fit values were used to correct to first order slight differences between printed and CAD dimensions and manufacture dimensionally accurate objects.

C. Electronics Characterization

The circuits were diagnosed using source-meter power supplies (Keithley 2657A, Tektronix, Inc., Beaverton, OR, USA) with 0.03% error when applying of measuring currents or voltages and a Rigol[1] DS6104 Digital Oscilloscope (Rigol, Portland, OR, USA) with 0.5% measurement error.

The implemented QMF driving circuit is composed of five subcircuits (see Fig. 7): 1) an ESP32 microcontroller board; 2) a buffer board; 3) a full-bridge board; 4) an RLC transformer network; and 5) a buck-boost power supply; an early, piecewise version of the circuit is shown in Fig. 8. The overarching circuit flow is as follows: 1) a square wave of specific frequency is generated and amplified; 2) the square wave interfaces with an IC to control four MOSFETS (full bridge) that send current across a transformer network that

[1]Registered trademark.

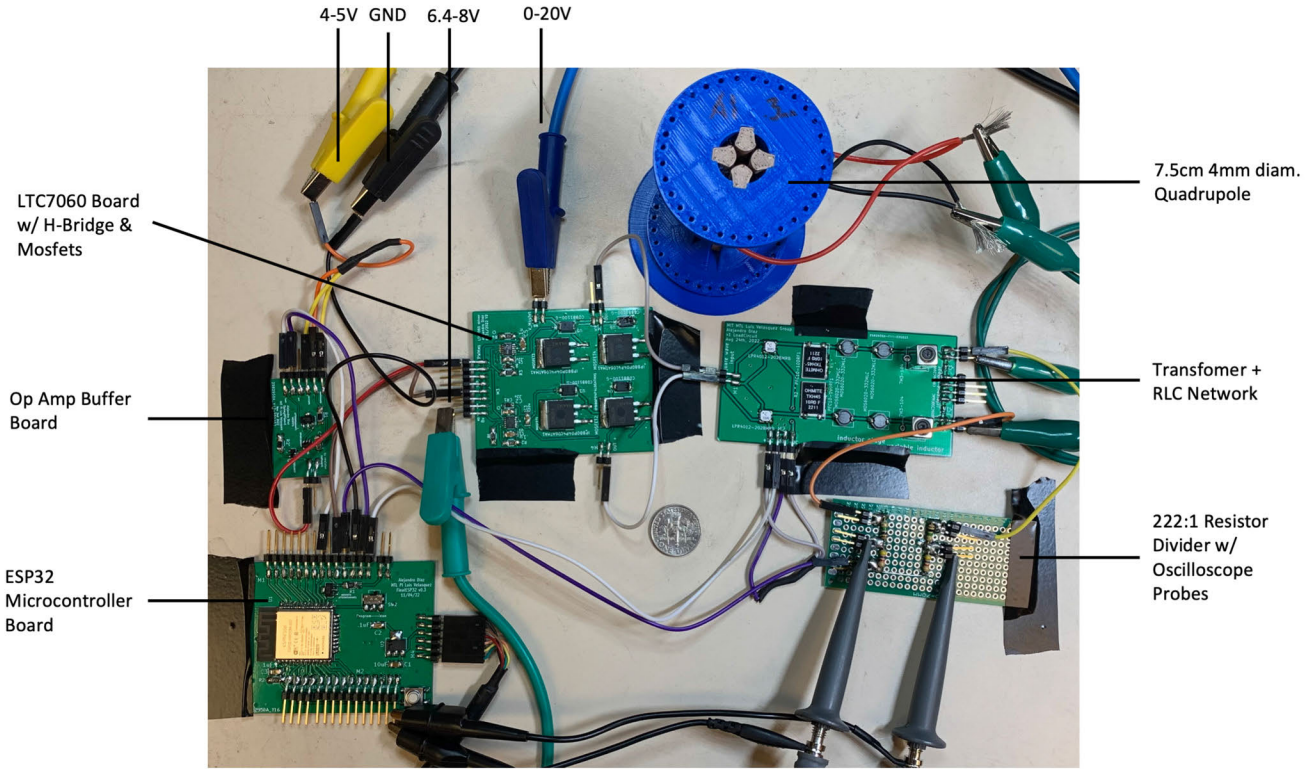

Fig. 8. Early, piecewise version of the QMF driving circuit next to a U.S. dime coin for comparison. The overall dimensions of the microcontroller board and the buffer board are 80 × 75 × 7 mm and 20 × 70 × 7 mm, respectively. The overall dimensions of the transformer board and the MOSFET board are 100 × 60 × 15 mm and 85 × 90 × 7 mm, respectively. The four subcircuits weigh combined 70 g. The setup also uses commercial three buck-boost converters as power supply occupying a volume of 100 × 75 × 20 mm and weighting 120 g.

both amplifies the signal and splits it into two 180°, out-of-phase square waves; and 3) finally, two identical tuned RLC circuits (operating at their resonant frequency) filter and amplify the square waves into sinusoidal waves across the QMF.

The following is a more detailed description of the circuit developed to drive the QMFs. The ESP32 microcontroller board [see Fig. 9(a)] creates a square wave that switches at the desired frequency. The buffer board [see Fig. 9(b)] takes the generated square wave from the ESP32 and feeds it into the LTC7060 board [see Fig. 9(c)]. The LTC7060 circuit interfaces with the full bridge [see Fig. 9(d)] that controls four MOSFETs. The MOSFETs are turned on and off in pairs to "push and pull" current across the load. In this case, the load is a symmetric transformer and *RLC* network [see Fig. 9(e)] that power the QMF. The MOSFETs supply a square wave to the two identical transformers; however, they are referenced to differing dc voltages and are reversed, such that the outputs of the transformers are 180° out-of-phase from each other. The amplified, out-phase square waves are converted into high-amplitude, sinusoidal waves by two identical, at resonance RLC circuits. The resulting sinusoids are directly applied to the electrodes of the QMF. The circuitry also contains ground planes to reduce noise and interfering signals. The circuit is capable of supplying RF voltages between 0 V and 400 V_{pp} with dc offsets required by the Mathieu equation to set stable ion trajectories within the QMF. The circuit to drive the QMF consumes 786 mW of power to provide up to 448 V_{pp} signals (see Fig. 10)—well beyond the voltages required to drive the QMF to measure the ionosphere and well below the power available in a typical CubeSat [36]. The final circuit that combines the microcontroller, buffer, and MOSFET subcircuits is 55 × 125 × 7 mm. The buck-boost converters used in this study were off-the-shelf items (TPS55289 Buck-Boost Converter Evaluation Board, Texas Instruments, Dallas, TX, USA). The fast Fourier transform (FFT) of the signal generated by the circuit shows no spurious harmonics, evidencing the circuit generates a pure sinusoidal signal (see Fig. 11).

There are several suggested directions to improve the QMF driving circuit. First, we used an off-the-shelf, variable buck-boost converter; it is possible to develop a custom converter to further reduce the power consumption and volume. Second, implementing negative feedback for the dc and RF amplitudes would make the system more precise. Third, control of the ionizer (if the MS is intended to characterize neutral species of the ionosphere), ion optics, and a current detector would be necessary to have a fully contained MS solution. Finally, the circuitry developed in this study is not space compatible; however, if the circuitry was encased in an aluminum enclosure about 7 mm thick, the circuitry would be space compatible with regard to radiation for missions, such as going to the moon or Mars [37]. The design of the CubeSat will strongly influence how this would be accomplished.

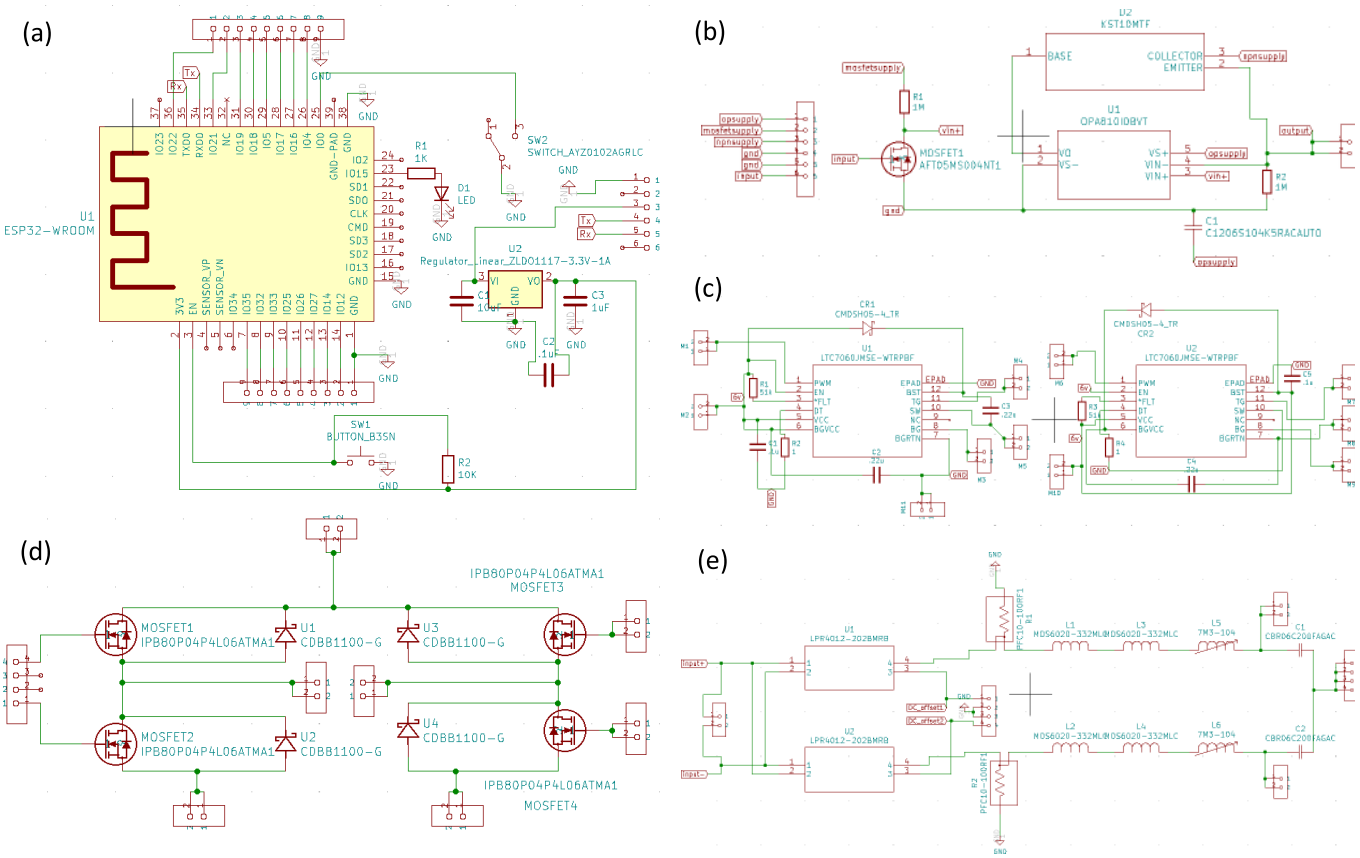

Fig. 9. Subcircuits used to drive the 3-D-printed QMFs. (a) Schematic of the ESP32 driving electronics, (b) schematic of buffer board, (c) LTC7060 board, (d) H-bridge MOSFET board, and (e) parallel transformers to RLC network and load capacitors that simulate the capacitive load of a quadrupole.

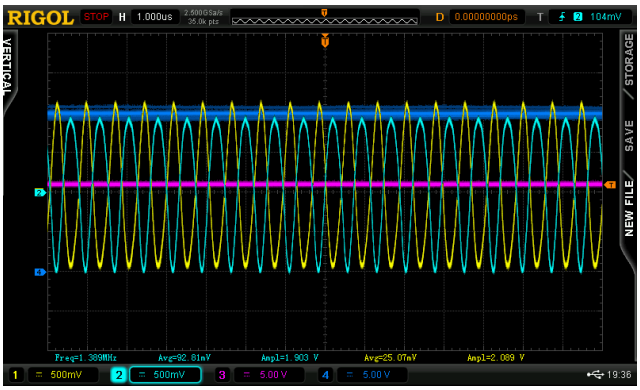

Fig. 10. Oscilloscope screenshot showing the 448-V_{pp} RF sinusoidal waves (yellow and teal curves) that are produced by the circuit while consuming 786 mW. Blue line is the dc offset. Magenta line is the dc sinusoidal amplitude voltage supply. Sinusoidal waves are measured across the quadrupole with a 224:1 resistor network. The error of the oscilloscope measurements is 0.5%.

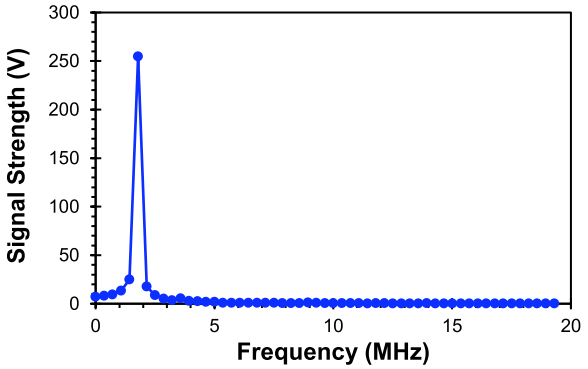

Fig. 11. FFT of the signal generated by the circuit. The data evidence that the circuit produces a pure sinusoidal wave. The error of the signal strength measurements is 0.5%.

D. QMF Characterization

The QMFs were tested in a vacuum chamber (Kurt Lesker, Jefferson Hills, PA, USA) pumped down by a dry rough pump (Adixen ACP 15, Pfeiffer, Annecy, France) and a turbomolecular pump (HiPace 300 Turbo TC400, Pfeiffer Vacuum Inc., Nashua, NH, USA); the chamber had a base pressure equal to 4×10^{-8} Torr. The QMF was connected to a commercial thermionic electron impact gas ionizer (Ardara Technologies Slimline, Ardara Technologies LP, Ardara, PA, USA) and a Faraday plate as a detector (see Fig. 12). Argon was introduced to the chamber using a leak valve, reaching a pressure equal to 2.7×10^{-4} Torr. Ions were created with an energy equal to 9.8 eV. Ar is commonly used for benchmarking mass filters because it has a large electron impact ionization cross-section, making it easier to ionize versus other gas species. Also, although it would be simple to leak air into the vacuum chamber, unlike air (oxygen), Ar does not degrade the thermionic filament of the electron impact ionizer, making it possible to ionize the gas at high pressure (0.1 mTorr) without degrading the ionizer. In addition, the ionosphere is mostly composed of N_2, O_2, O, H, He, and Ar [30]; the heaviest species of the set is Ar (40 Da); therefore, measuring the other gases would

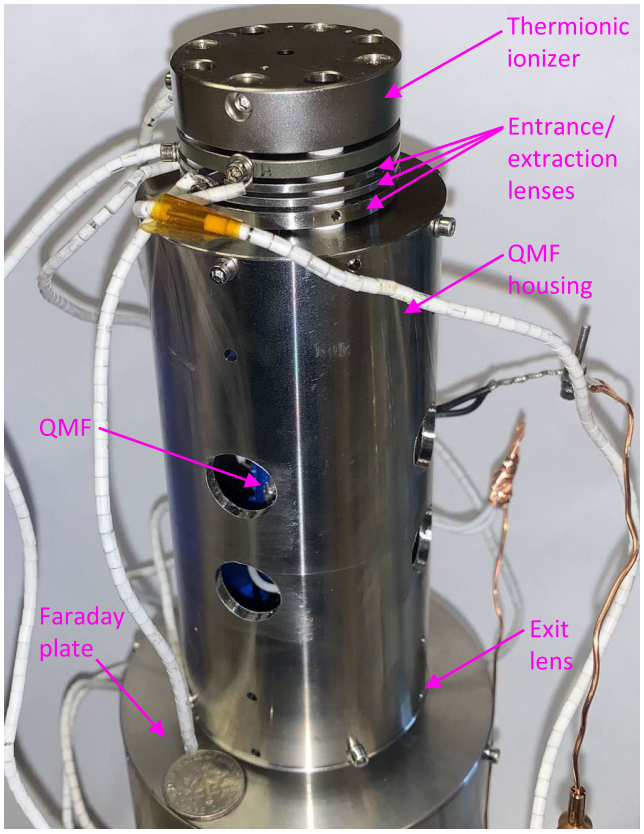

Fig. 12. QMF connected to commercial housing, ionizer, ion optics, and detector next to a U.S. dime coin as comparison. There is an Einzel lens within the metal housing (between the QMF and the entrance lens) that focuses and collimates the ion beam getting into the QMF.

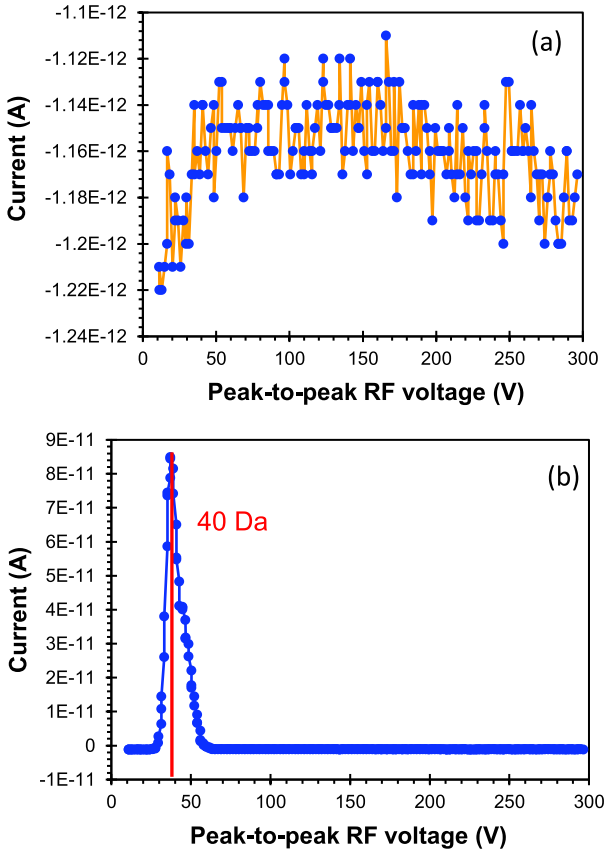

Fig. 13. Collector current versus peak-to-peak RF bias voltage with (a) ionizer off and (b) ionizer on. Red line indicates the expected peak of 40 Da according to the Mathieu equation. The QMF data show a mass scanning of up to 300 Da. The error in the measured/applied currents and voltages is 0.03%.

require applying lower voltages [as shown by (2) and (3), there is a linear relationship between the amplitude of the voltages and the mass of the ions transmitted by the quadrupole].

With the QMF voltages ON and the ionizer OFF, the Faraday cup detected noise currents on the order of $\sim 1.15 \times 10^{-12}$ A [see Fig. 13(a)]. With the ionizer ON and the QMF sinusoidal voltages ON at 1.34 MHz, the detector correctly generates the mass spectra of Ar (40 Da) with a peak intensity almost two orders of magnitude larger than the noise floor [see Fig. 13(b)]. The Ar peak matches the predicted value from the Mathieu equation. The resolution R of a quadrupole is given by

$$R = \frac{m}{\Delta m} \tag{6}$$

where m is the peak mass and Δm is the peak mass width, typically the full-width at half-maximum (FWHM). The resolution benchmarks the ability of the quadrupole to distinguish adjacent peaks. The resolution of the Ar peak is equal to 5. A summary of the results of this study and the literature is provided in Table II. The resolution attained by our QMFs is comparable to those reported from 3-D printed QMFs, far more considering that those devices operate at larger RF frequencies and $R \propto f^2$ [1]. For example, Szyszka et al. [20] reported a miniaturized, 3-D-printed QMF that attains a resolution of 9 at 28 Da while operating at 6 MHz. Also, Brkić et al. [21] reported 3-D-printed quadrupoles with resolution equal to 7 at 2 Da for similar transmitted ion currents while operating at 3.68 MHz. Nonetheless, to the best of our knowledge, the QMFs reported in this study are the first monolithically and entirely made via 3-D printing.

TABLE II
SUMMARY OF SPECIFICATIONS AND PERFORMANCE OF REPORTED, MINIATURIZED QMFS

Ref.	R (-)	r_o (μm)	L (mm)	f (MHz)
[39]	32 @ 40 Da	217	30	6
[7]	70 @ 28 Da	690	90	2
[38]	200 @ 219 Da	217	30	6
[13]	40 @ 40 Da	707	30	4
[20]	11 @ 28 Da	870	70	3.5
[21]	7 @ 2 Da	2000	50	3.69
This work	5 @ 40 Da	2000	75	1.34

The resolution of our QMFs is over an order of magnitude smaller than reported nonprinted, miniaturized quadrupoles. For example, Geear et al. [38] reported miniaturized quadrupoles with a resolution of 200 at 200 Da while

operating at 6 MHz, Velásquez-García et al. [7] reported QMFs with a resolution of 70 at 28 Da while operating at 2 MHz, Cheung et al. [13] reported a resolution of 40 at 40 Da while operating at 4 MHz, and Taylor et al. [39] demonstrated QMFs with 32 resolution at 40 Da while operating at 6 MHz. Nevertheless, these devices were made using semiconductor cleanroom technology, which is expensive, time-consuming, and incompatible with in-space manufacturing. Moreover, these QMFs were run with bulky electronics. In contrast, the 3-D-printed QMFs reported in this study are over an order of magnitude cheaper (each costs about U.S. $100 in materials) and over two orders of magnitude faster to make (it takes about 8 h to print one of them) and are compatible with in-space manufacturing (there are working extrusion 3-D-printers installed in the International Space Station [40]), and they include QMF driving electronics compatible with the size and power available in a 6U CubeSat. In addition, our 3-D-printed QMFs are disposable during reentry as they are made of polymer. It might be possible to increase the resolution of our QMFs by increasing the RF frequency and/or the length L of the devices as $R \propto f^2 L^2$ [9]. Given the constraints in size and weight imposed by CubeSats, implementing driving circuits with a larger RF frequency is a more desirable approach, although this requires the use of larger bias voltages and a redesign of the electronics. A further reduction of the electrode in-plane dimensions using the same electrically conductive feedstock is possible if the RF frequency is increased and still be able to contain the RF wave.

V. Conclusion

This study reported the first proof-of-concept demonstration of monolithically 3-D-printed, hyperbolic, compact RF QMFs for CubeSat MS. The devices are fabricated via multimaterial extrusion using doped and undoped PLA. The work also included the development of compact electronics to drive the QMFs that are compatible with the size, weight, and power constraints of CubeSats. Mass spectra for Ar (a representative gas found in the ionosphere) were successfully obtained.

There are several possible directions for extending the work. Regarding the manufacturing of the QMF, extrusion 3-D printing has accuracy limitations compared to other AM techniques, e.g., vat photopolymerization. However, most 3-D printing techniques do not have the capability to monolithically create multimaterial objects. Also, the plating of the conductive structures in the QMF might improve the performance of the QMF by making the electrodes significantly more electrically conductive. In terms of the QMF hardware, it might be possible to monolithically integrate the ion optics with the QMF to better control the ions into and out of the quadrupole.

Tentative directions to improve the QMF driving electronics include adding feedback for the voltage amplitudes to more accurately control the voltages, adding more filtering/shielding to produce sine waves with less harmonics, and involving more power saving techniques, both in code and in the physical printed circuit board (PCB). To send the electronics to space, future work will have to interface the microcontroller with other electronics/power supplies onboard the satellite, looking to make the electronics more compact. The buck-boost power supplies used in this study have many test points and prototyping features, and thus, the footprint and weight can be greatly reduced. The other electronics required to have a working, compact mass spectrometer, e.g., ionizer, detector, should also be developed.

There are also alternate methods of driving a QMF that might yield better performance. For example, instead of varying the RF amplitudes, the frequency can be varied to achieve the same mass spectrum scanning [41], which would heavily reduce the RF amplitude requirement and could work readily with our system, given that the electronics can control the driving frequency via code. There are also alternate stability regions to operate within that should achieve higher resolution at the expense of more power [42]. Additionally, further improving the printing setup and experimenting with more conductive filaments or plating the electrodes could tentatively yield QMFs with higher resolution.

References

[1] J. H. Gross, *Mass Spectrometry*. Cham, Switzerland: Springer, 2017.

[2] C. D. Mowry, R. L. Jarek, J. Román-Kustas, A. C. Telles, and A. S. Pimentel, "Gas analysis by mass spectrometry," in *ASM Handbook*. Park, OH, USA: ASM International, 2019, pp. 143–152, doi: 10.31399/asm.hb.v10.a0006663.

[3] Z. Yang et al., "Review and prospect on portable mass spectrometer for recent applications," *Vacuum*, vol. 199, May 2022, Art. no. 110889, doi: 10.1016/j.vacuum.2022.110889.

[4] F. Yan et al., "A newly developed prototype magnetic sector mass spectrometer with high resolving power," *J. Instrum.*, vol. 4, Jan. 2019, Art. no. P01025, doi: 10.1088/1748-0221/14/01/P01025.

[5] J. Sun et al., "Miniaturized time-of-flight mass spectrometer for lunar water detection," *Vacuum*, vol. 204, no. 5, 2022, Art. no. 111312, doi: 10.1016/j.vacuum.2022.111312.

[6] Z. Ouyang et al., "Rectilinear ion trap: Concepts, calculations, and analytical performance of a new mass analyzer," *Anal. Chem.*, vol. 76, no. 16, pp. 4595–4605, 2004, doi: 10.1021/ac049420n.

[7] L. F. Velásquez-García, K. Cheung, and A. I. Akinwande, "An application of 3-D MEMS packaging: Out-of-plane quadrupole mass filters," *J. Microelectromech. Syst.*, vo. 16, no. 6, pp. 1430–1438, Dec. 2008, doi: 10.1109/JMEMS.2008.2006769.

[8] P. Mielczarek, J. Silberring, and M. Smoluch, "Miniaturization in mass spectrometry," *Mass Spectrometry Rev.*, vol. 39, nos. 5–6, pp. 453–470, Sep. 2020, doi: 10.1002/mas.21614.

[9] R. R. A. Syms and S. Wright, "MEMS mass spectrometers: The next wave of miniaturization," *J. Micromech. Microeng.*, vol. 26, no. 2, 2016, Art. no. 023001, doi: 10.1088/0960-1317/26/2/023001.

[10] R. E. March, "An introduction to quadrupole ion trap mass spectrometry," *J. Mass Spectrometry*, vol. 32, no. 4, pp. 351–369, Apr. 1997, doi: 10.1002/(SICI)1096-9888(199704)32:4<351::AID-JMS512>3.0.CO;2-Y.

[11] S. Boumsellek and R. J. Ferran, "Trade-offs in miniature quadrupole designs," *J. Amer. Soc. Mass Spectrometry*, vol. 12, no. 6, pp. 633–640, 2001, doi: 10.1016/S1044-0305(01)00248-3.

[12] B. Brkić, N. France, S. Giannoukos, and S. Taylor, "An optimised quadrupole mass spectrometer with a dual filter analyser for in-field chemical sniffing of volatile organic compounds," *Analyst*, vol. 143, no. 15, pp. 3722–3728, 2018, doi: 10.1039/C8AN00862K.

[13] K. Cheung, L. F. Velásquez-García, and A. I. Akinwande, "Chip-scale quadrupole mass filters for portable mass spectrometry," *J. Microelectromech. Syst.*, vol. 19, no. 3, pp. 469–483, Jun. 2010, doi: 10.1109/JMEMS.2010.2046396.

[14] S. Wright et al., "A microelectromechanical systems-enabled, miniature triple quadrupole mass spectrometer," *Anal. Chem.*, vol. 87, no. 6, pp. 3115–3122, 2015, doi: 10.1021/acs.analchem.5b00311.

[15] B. A. Praveena et al., "A comprehensive review of emerging additive manufacturing (3D printing technology): Methods, materials, applications, challenges, trends and future potential," *Mater. Today: Proc.*, vol. 53, no. 3, pp. 1309–1313, 2022, doi: 10.1016/j.matpr.2021.11.059.

[16] G. D. Goh et al., "Process–structure–properties in polymer additive manufacturing via material extrusion: A review," *Crit. Rev. Solid State Mater. Sci.*, vol. 45, no. 2, pp. 113–133, 2020, doi: 10.1080/10408436.2018.1549977.

[17] A. P. Taylor, J. I. Reyes, and L. F. Velásquez-García, "Compact, magnetically actuated, additively manufactured pumps for liquids and gases," *J. Phys. D, Appl. Phys.*, vol. 53, no. 35, 2020, Art. no. 355002, doi: 10.1088/1361-6463/ab8de8.

[18] F. Li, N. P. Macdonald, R. M. Guijt, and M. C. Breadmore, "Increasing the functionalities of 3D printed microchemical devices by single material, multimaterial, and print-pause-print 3D printing," *Lab a Chip*, vol. 19, no. 1, pp. 35–49, 2019, doi: 10.1039/c8lc00826d.

[19] A. P. Taylor and L. F. Velásquez-García, "Miniaturized diaphragm vacuum pump by multi-material additive manufacturing," *J. Microelectromech. Syst.*, vol. 26, no. 6, pp. 1316–1326, Dec. 2017, doi: 10.1109/JMEMS.2017.2743020.

[20] P. Szyszka, J. Jendryka, M. Bialas, and T. Grzebyk, "Towards 3D printed compact quadrupole mass spectrometer with MEMS components," in *Proc. IEEE 20th Int. Conf. Micro Nanotechnol. Power Gener. Energy Convers. Appl. (PowerMEMS)*, Exeter, United Kingdom, Dec. 2021, pp. 144–147, doi: 10.1109/PowerMEMS54003.2021.9658391.

[21] B. Brkić et al., "Development of quadrupole mass spectrometers using rapid prototyping technology," *J. Amer. Soc. Mass Spectrometry*, vol. 20, no. 7, pp. 1359–1365, 2009, doi: 10.1016/j.jasms.2009.03.025.

[22] G. P. Sutton and O. Biblarz, *Rocket Propulsion Elements*, 9th ed. Hoboken, NJ, USA: Wiley, 2017.

[23] W. Moore, "On the motion of rockets both in nonresisting and resisting mediums," *J. Natural Philosophy, Chem. Arts*, vol. 27, pp. 276–285, Jan. 1810.

[24] H. W. Jones, "The recent large reduction in space launch cost," in *Proc. 48th Int. Conf. Environ. Syst. (ICES)*, Albuquerque, NM, USA, 2018, pp. 2018–2081.

[25] M. Hirsch et al., "Enablement of scientific remote sensing missions with in-space 3D printing," in *Proc. SPIE*, vol. 9854, 2016, Art. no. 985413, doi: 10.1117/12.2223467.

[26] V. V. Svotina and M. V. Cherkasova, "Space debris removal—Review of technologies and techniques. Flexible or virtual connection between space debris and service spacecraft," *Acta Astronautica*, vol. 204, pp. 840–853, Mar. 2023.

[27] *NASA and Japan to Launch World's 1st Wooden Satellite as Soon as 2024. Why?* Accessed: Mar. 7, 2024. [Online]. Available: https://www.livescience.com/space/space-exploration/nasa-and-japan-to-launch-worlds-1st-wooden-satellite-as-soon-as-2024-why

[28] A. Diaz and L. F. Velásquez–García, "Miniature, 3-D printed RF quadrupole mass filters for cubesats," in *Proc. IEEE 36th Int. Vac. Nanoelectronics Conf. (IVNC)*, Cambridge, MA, USA, Jul. 2023, pp. 106–108, doi: 10.1109/IVNC57695.2023.10188995.

[29] D. J. Gershman et al., "Comparing the performance of hyperbolic and circular rod quadrupole mass spectrometers with applied higher order auxiliary excitation," *Int. J. Mass Spectrometry*, vols. 319–320, pp. 17–24, May 2012.

[30] L. F. Velásquez–García, J. Izquierdo-Reyes, and H. Kim, "Review of in-space plasma diagnostics for studying the Earth's ionosphere," *J. Phys. D, Appl. Phys.*, vol. 55, no. 26, 2022, Art. no. 263001, doi: 10.1088/1361-6463/ac520a.

[31] E. G. Kilinc, K. Ture, F. Maloberti, and C. Dehollain, "Design and comparison of class-C and class-D power amplifiers for remotely powered systems," in *Proc. IEEE 20th Int. Conf. Electron., Circuits, Syst. (ICECS)*, Abu Dhabi, United Arab Emirates, Dec. 2013, pp. 461–464, doi: 10.1109/ICECS.2013.6815454.

[32] *Electrifi FAQ*. Accessed: Mar. 7, 2024. [Online]. Available: https://www.multi3dllc.com/faqs/

[33] Z. Sun and L. Fernando Velásquez-García, "Monolithic FFF-printed, biocompatible, biodegradable, dielectric-conductive microsystems," *J. Microelectromech. Syst.*, vol. 26, no. 6, pp. 1356–1370, Dec. 2017, doi: 10.1109/JMEMS.2017.2746627.

[34] P. F. Flowers, C. Reyes, S. Ye, M. J. Kim, and B. J. Wiley, "3D printing electronic components and circuits with conductive thermoplastic filament," *Additive Manuf.*, vol. 18, pp. 156–163, Dec. 2017, doi: 10.1016/j.addma.2017.10.002.

[35] T. J. Colvin, J. Karcz, and G. Wusk, *Cost and Analysis of Orbital Debris Remediation*, National Aeronautics and Space Administration, Office of Technology, Policy, and Strategy, Document 20230002817, 2023.

[36] A. Edpuganti et al., "A comprehensive review on CubeSat electrical power system architectures," *IEEE Trans. Power Electron.*, vol. 37, no. 3, pp. 3161–3177, Mar. 2022, doi: 10.1109/TPEL.2021.3110002.

[37] A. Märki, "Radiation analysis for moon and Mars missions," *Int. J. Astrophys. Space Sci.*, vol. 8, no. 3, pp. 16–26, 2020, doi: 10.11648/j.ijass.20200803.11.

[38] M. Geear, R. R. A. Syms, S. Wright, and A. S. Holmes, "Monolithic MEMS quadrupole mass spectrometers by deep silicon etching," *J. Microelectromech. Syst.*, vol. 14, no. 5, pp. 1156–1166, Oct. 2005, doi: 10.1109/JMEMS.2005.851799.

[39] S. Taylor, R. F. Tindall, and R. R. A. Syms, "Silicon based quadrupole mass spectrometry using microelectromechanical systems," *J. Vac. Sci. Technol. B, Microelectron. Nanometer Struct. Process., Meas., Phenomena*, vol. 19, no. 2, pp. 557–562, 2001, doi: 10.1116/1.1359172.

[40] T. Prater et al., "3D printing in zero G technology demonstration mission: Complete experimental results and summary of related material modeling efforts," *Int. J. Adv. Manuf. Technol.*, vol. 101, pp. 391–417, Nov. 2019, doi: 10.1007/s00170-018-2827-7.

[41] B. Wilamowski et al., "Enhancing the sensitivity of miniaturized quadrupole mass spectrometers," in *Proc. 27th Annu. Conf. IEEE Ind. Electron. Soc. (IECON)*, Denver, CO, USA, 2001, pp. 147–152, vol. 1, doi: 10.1109/IECON.2001.976470.

[42] D. J. Gershman et al., "Higher order parametric excitation modes for spaceborne quadrupole mass spectrometers," *Rev. Sci. Instrum.*, vol. 82, no. 12, 2011, Art. no. 125109, doi: 10.1063/1.3669781.

Alejandro Diaz received the B.S. and M.Eng. degrees from the Department of Electrical Engineering and Computer Science, Massachusetts Institute of Technology, Cambridge, MA, USA, in 2021 and 2023, respectively.

His work interests span sensor implementation, sustainability in the modern age, and hardware/software integration.

Luis Fernando Velásquez-García (Senior Member, IEEE) received the Mechanical Engineer and Civil Engineer degrees (magna cum laude and valedictorian of the School of Engineering in both cases) from the Universidad de Los Andes, Bogotá, Colombia, in 1998 and 1999, respectively, and the M.S. and Ph.D. degrees from Massachusetts Institute of Technology (MIT), Cambridge, MA, USA, in 2001 and 2004, respectively.

In 2004, after completing his studies, he became a Post-Doctoral Associate with the Microsystems Technology Laboratories (MTL), MIT, where he was appointed as a Research Scientist in 2005. Since 2009, he has been a Principal Scientist and a Core Member with MTL. He is an expert in micro and nanofabrication technologies. He leads the Micro- and Nano-enabled Multiplexed Scaled-Down Systems Group, MIT, which conducts fundamental and applied research on miniaturized devices and systems that exploit high-electric field phenomena (e.g., electrospray, gas ionization, field emission, X-rays, and plasmas) for space, energy, healthcare, manufacturing, and analytical applications. Currently, his work focuses on additively manufactured micro and nanosystems. He has authored more than 66 journal publications and 103 conference proceedings publications, and he is the holder of 16 patents on microelectromechanical systems (MEMS)/nanoelectromechanical systems (NEMS) technologies.

Dr. Velásquez-García is a Full Member of Sigma Xi and a Senior Member of the American Institute of Aeronautics and Astronautics (AIAA). He served as the Co-Chair of the 15th International Conference on Micro and Nanotechnology for Power Generation and Energy Conversion Applications (PowerMEMS 2015) and as the Chair of the 36th International Vacuum Nanoelectronics Conference (IVNC 2023). He is currently the Vice President (VP) of Finance of the IEEE MEMS Technical Community. His group's work has received multiple recognitions, including best paper awards in conferences such as PowerMEMS and Transducers, and best-paper highlights at journals, such as the IEEE JOURNAL OF MICROELECTROMECHANICAL SYSTEMS, the *IOP Journal of Physics D: Applied Physics*, the *IOP Journal of Micromechanics and Microengineering*, and *IOP Nanotechnology*.